

pubs.acs.org/est Article

Degradation Kinetics of Antibiotic Resistance Gene *mecA* of Methicillin-Resistant *Staphylococcus aureus* (MRSA) during Water Disinfection with Chlorine, Ozone, and Ultraviolet Light

Yegyun Choi, Huan He, Michael C. Dodd, and Yunho Lee*



Cite This: https://dx.doi.org/10.1021/acs.est.0c05274



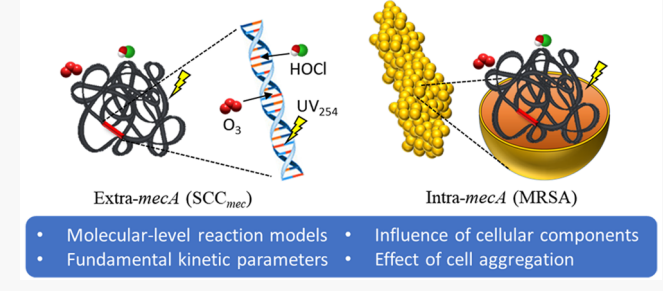
ACCESS

Metrics & More

Article Recommendations

Supporting Information

ABSTRACT: Degradation kinetics of antibiotic resistance genes (ARGs) by free available chlorine (FAC), ozone (O_3) , and UV_{254} light (UV) were investigated in phosphate buffered solutions at pH 7 using a chromosomal ARG (mecA) of methicillin-resistant Staphylococcus aureus (MRSA). For FAC, the degradation rates of extracellular mecA (extra-mecA) were accelerated with increasing FAC exposure, which could be explained by a two-step FAC reaction model. The degradation of extra-mecA by O_3 followed second-order reaction kinetics. The degradation of extra-mecA by UV exhibited tailing kinetics, which could be described by a newly proposed kinetic model considering cyclobutane pyrimidine dimer



(CPD) formation, its photoreversal, and irreversible (6–4) photoproduct formation. Measured rate constants for extra-mecA increased linearly with amplicon length for FAC and O₃, or with number of intrastrand pyrimidine doublets for UV, which enabled prediction of degradation rate constants of extra-mecA amplicons based on sequence length and/or composition. In comparison to those of extra-mecA, the observed degradation rates of intracellular mecA (intra-mecA) were faster for FAC and O₃ at low oxidant exposures but significantly slower at high exposures for FAC and UV. Differences in observed extra- and intracellular kinetics could be due to decreased DNA recovery efficiency and/or the presence of MRSA aggregates protected from disinfectants.

■ INTRODUCTION

Increasing antibiotic resistance is a growing public health issue worldwide, as it has lowered the therapeutic efficacy of antibiotics. Rising antibiotic resistance is typically associated with overuse and misuse of antibiotics in healthcare or agricultural practice, which can select antibiotic resistant bacteria (ARB) carrying genes (ARGs) responsible for antibiotic resistance traits. Bacteria can also share mobile ARGs in forms of plasmids, chromosomal DNA, and bacteriophages through horizontal gene transfer (HGT) processes, leading to the dissemination of antibiotic resistance among bacterial populations.

Notably, ARB and ARGs are recognized to be widespread in various aquatic environments.^{5–8} This has raised additional concerns that their presence may promote the dissemination of antibiotic resistance via anthropogenic and natural water cycles, and eventually to pathogenic bacteria.^{9,10} In this context, ARGs are now considered as a type of water contaminant.⁵

Disinfection of drinking water and wastewater effluent can provide an important barrier to the spread of pathogenic microorganisms in urban water cycles. ¹¹ Chlorine, ozone (O_3) , and ultraviolet light (UV) are widely used as disinfectants. ¹² There has been growing interest in the efficacy of water disinfection processes to control dissemination of ARB and

ARGs. 13-15 Studies have shown that water disinfection processes generally decrease the absolute levels of ARB, whereas increases in the *relative* proportions of specific ARB (or associated ARGs) among surviving bacteria (or gene pools) are sometimes observed, suggesting possible selection for ARB. 16-19 Significant reductions in the absolute concentrations of ARGs have also been observed, though their removal efficacies have been found to vary widely depending on the specific ARG, analytical method used (e.g., qPCR vs culture-based assay), length of amplicon target monitored (qPCR), process operational conditions (e.g., disinfectant exposure), and also in some cases whether the ARG is extracellular vs intracellular or plasmid-borne vs chromosomal. $^{16,17,20-24}$ In order to enable intercomparison and generalization of ARG removal efficacy, it is thus necessary to elucidate and determine the fundamental kinetic parameters and reactions governing ARG degradation by water disinfectants. Only a limited number of studies have reported

Received: August 6, 2020 Revised: January 8, 2021 Accepted: January 8, 2021



such fundamental kinetic parameters (e.g., bimolecular or UV fluence-based rate constants) or evaluated molecular-level reaction models for the degradation of plasmid- $^{25-28}$ or chromosome-encoded ARGs 29 by water disinfectants.

This study investigated the degradation kinetics of the chromosome-encoded ARG mecA during treatment with free available chlorine (FAC), O₃, and UV (254 nm) in bench-scale experiments. Methicillin-resistant Staphylococcus aureus (MRSA) and mecA, responsible for methicillin resistance in MRSA strains, have been detected in municipal wastewaters30-33 and are considered as an ARB and ARG of significant concern, respectively, due to the former's widespread occurrence as an opportunistic pathogen and the latter's possible contributions to antibiotic resistance dissemination among methicillin-susceptible strains of Staphylococci by HGT. 34-36 Although degradation of *mecA* by UV and FAC has previously been investigated, detailed kinetic information has not yet been reported. ^{20,24} The *mecA* for this study was derived from a clinically relevant, multidrug-resistant MRSA strain³⁷ and is contained on the staphylococcal cassette chromosome mec (SCCmec) as a mobile genetic element.³ Degradation kinetics of both extra- and intracellular forms of mecA were investigated here in order to examine the influence of cellular components and/or cell aggregation on mecA degradation kinetics. Changes in cellular parameters such as culturability, membrane damage, and severe DNA damage were also determined, in order to evaluate the sequence of damage to cellular components during MRSA inactivation. Degradation of mecA was quantified using qPCR targeting a set of amplicons (212, 612, and 1018 bp) located within the full mecA gene. The observed kinetics were used to derive kinetic models and corresponding rate constants for each disinfectant, which were then compared to available literature values (noting that comparisons of FAC and O₃ data were limited to the chromosomal blt gene of Bacillus subtilis,²⁹ as directly comparable kinetics parameters are thus far available only for this gene). These findings were then evaluated with respect to their utility in predicting the degradation efficiency of mecA and potentially other ARGs (or any other segments of doublestranded DNA) during municipal water disinfection.

MATERIALS AND METHODS

Standards and Reagents. All chemicals (of at least reagent-grade purity) and media (certified-nuclease free) were purchased from commercial suppliers. Further details of the preparation of the disinfectants and culture media can be found elsewhere ^{27,38} and are also described in SI-Text-1.

Bacterial Strains. MRSA strain ATCC BAA-1556 (FPR3757) (*Staphylococcus aureus subsp.*)³⁷ was obtained from the American Type Culture Collection (ATCC). The strain was grown and harvested according to ATCC instructions (SI-Text-2).³⁹ Genomic DNA of BAA-1556 has been fully sequenced (NCBI,GeneBank:CP000255.1) and contains SCC*mec* type IV, within which the *mecA* gene is located.⁴⁰

DNA Extraction. High molecular weight chromosomal DNA (4–20 kbp) was extracted from BAA-1556 cells with FastDNA spin kits for soil (MP Biomedicals,USA). After the extractions, DNA was further purified with an ethanol precipitation. Phenol-chloroform-isoamyl alcohol (PCI) DNA extraction was used as an alternative extraction method in a few selected experiments for evaluating DNA recovery from chlorinated MRSA. Quality and concentration of purified DNA

were checked with a NanoDrop 2000 Spectrophotometer (Thermo Scientific, USA) or fluorescence-based DNA quantification kit (DNAQF, Sigma, USA). Further details are provided in SI-Text-3.

Treatment of Extracellular ARGs. Extracted DNA from MRSA (30–60 ng/ μ L, extracellular ARG) was diluted to 10⁶ copy/ml (= 1.2 × 10⁻² μ g/mL) in pH 7, 10 mM phosphate buffer solution and treated with each disinfectant. The applied initial *mec-A* concentration was chosen to allow observation of *mec-A* degradation of more than 4 logs decrease in concentration. The reaction temperature was 20(±1)°C for FAC and O₃, and 22(±2)°C for UV. FAC experiments were also conducted at different pH and temperatures.

FAC and O₃ treatments were performed in batch reactors by adding FAC (~30 mM) and O₃ (~1 mM) stock solutions to 100 mL buffer solutions containing the DNA under stirred mixing to yield target concentration ranges of 70-280 µM for FAC and 2.6-10.4 μ M for O₃. The O₃ reactions were performed with/without tert-butanol (50 mM) as OH scavenger. At selected times after disinfectant addition-from 0-100 min for FAC and 0-45 s for O₃, 1 mL volumes of the reaction solutions were collected and quenched (5-fold molar excess relative to disinfectants) with thiosulfate stock (10 mM) for FAC, or with cinnamic acid stock (10 mM) for O₃. These samples were later used for qPCR analyses of extra-mecA amplicons. For FAC, time-dependent FAC concentrations (Figure S1) were determined using the ABTS colorimetric method.⁴³ Time-dependent O₃ concentrations (Figure S2) were determined from benzaldehyde formation in the cinnamic acid-quenched samples.44

UV irradiation was conducted in a quasi-collimated beam system equipped with a low-pressure Hg lamp emitting 254 nm light (Sankyo Denki Ltd., Tokyo, Japan). Sample solutions (100 mL) were placed in a crystallization dish with a diameter of 9 cm and a sample depth of 6 cm. The UV fluence rate was determined to be 0.3 mW/cm² using atrazine actinometry. Sample sample depth of 6 cm.

Treatment of MRSA Cells, Including Intracellular *mecA*. Cultured MRSA were diluted to 10^6 CFU/mL in phosphate buffer (10 mM) at pH 7 (in addition to pH 8.5 for FAC) and treated with each disinfectant, following the same protocols used for treating extra-ARGs. The treated cells were recovered by filtering samples (10 mL for FAC and 1 mL for O_3 and UV, respectively) through 0.45 μ m polycarbonate membranes (Whatman plc, GE) and processed for DNA extraction for determining the concentration of intracellular ARG. The treated MRSA cells were also analyzed in parallel for cell viability by a plate count method (SI-Text-2) and cellular component damages by flow cytometry methods (see below).

Quantitative Polymerase Chain Reaction (qPCR). qPCR analyses were performed using a CFX connect Real-Time PCR Detection System (Bio-Rad, USA). SsoFast EvaGreen Supermix (Bio-Rad, USA) was used as a qPCR reagent to quantify 212, 612, and 1018 bp amplicons targeting the *mecA* gene. The sequences and locations of the target amplicons are provided in Table S1. Primers purchased from a commercial supplier (Macrogen, Korea) were designed based on the *mecA* sequence, with qPCR temperature profiles as indicated in Table S2. Further details of the qPCR assay such as determination of limits of detection and amplification efficiencies are provided in Figure S3 and SI-Text-4.

Other Analytical Methods. Flow cytometry (FCM) with fluorescence staining was used for determining membrane-

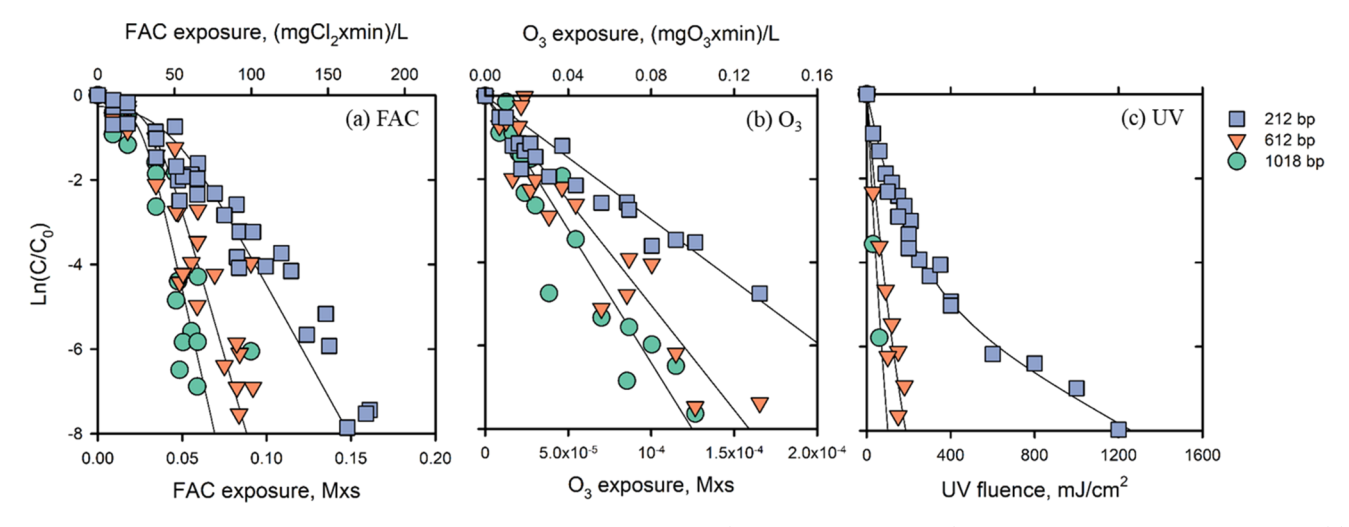


Figure 1. Logarithmic relative concentration of extra-mecA qPCR amplicons (212, 612, and 1018 bps) as a function of oxidant exposure for (a) FAC and (b) O₃, and UV fluence for (c) UV. For both FAC and O₃, extents of mecA degradation were expressed as a function of disinfectant exposures (= time-integrated disinfectant concentrations, Mxs). FAC exposures were calculated based on Figure S1a, and O₃ exposures were calculated based on Figure S2a. All data were obtained by treating extracellular DNA from MRSA BAA-1556 at pH 7 (10 mM phosphate buffer). In the case of O₃, tert-butanol (50 mM) was added to scavenge OH. Up to 8-ln reduction of the extra-mecA concentration could be quantified by the qPCR method under the tested experimental conditions. Symbols are the measured data and the lines are the linear/nonlinear regressions for rate constant determination (see the main text for the details of kinetic models).

intact cell counts (FCM-ICC), as well as total (including membrane-intact and membrane-compromised) cell counts without severe DNA damage (e.g., double-strand breakage) (FCM-TCC), using methods described in previous studies (SI-Text-5). Scanning electron microscopy (SEM) images of MRSA were determined using a Hitachi S-4700 (Hitachi, Japan), according to a previously reported sample preparation method (SI-Text-6), to investigate the possible influence of MRSA cell aggregates on intra-ARG degradation kinetics during FAC and UV treatment.

■ RESULTS AND DISCUSSION

Degradation Kinetics of extra-mecA. Figure 1 shows the logarithmic relative concentrations of the three qPCR amplicons as a function of disinfectant exposure or UV fluence during treatment of extra-mecA at pH 7 with (a) FAC, (b) O_3 , and (c) UV. For O_3 , tert-butanol (50 mM) was added to exclude *OH reactions. The FAC and O_3 treatments were performed at FAC concentrations of 5, 10, and 20 mg/L as Cl_2 and O_3 concentrations of 0.125, 0.25, and 0.5 mg/L. For both FAC and O_3 , extents of mecA degradation were dependent on oxidant exposures (= time-integrated oxidant concentrations) but were independent of the FAC (Figure S4) or O_3 concentrations (Figure S5) used to achieve a given oxidant exposure. Thus, pooled data for mecA degradation as a function of oxidant exposure (M × s) were used for kinetic analyses as shown in Figure 1 and other related Figures.

The degradation kinetics of extra-mecA by \underline{FAC} are described here (Figures 1a and S4). The degradation of mecA amplicons by FAC was relatively slow initially but became faster with increasing FAC exposure, exhibiting accelerating kinetics. After reaching a certain range of FAC exposure values (0.02–0.05 M \times s), the logarithmic-scale degradation of the amplicons became linear with respect to the FAC exposure. The degradation rate was lowest for the 212 bp, followed by the 612 bp and then the 1018 bp amplicons. The observed kinetics could be described by a sequential, two-step

reaction model originally proposed by He et al. $(2019)^{29}$ (eqs 1 and 2)

$$Amp + FAC \underset{Na_2S_2O_3}{\overset{k_{FAC,Amp}}{\longleftarrow}} Amp_{N-Cl}$$
 (1)

$$Amp_{N-Cl} + FAC \xrightarrow{k_{FAC,AmpN-Cl}} Product$$
 (2)

N-chlorination of nucleotide bases is the first step of the two-step FAC reaction model, forming a chlorinated amplicon (Amp_{N-Cl}) in eq 1, which can be reverted into the parent form upon its reaction with a strong reductant such as thiosulfate (reversible N-chlorination). Each N-chlorination of a nucleotide causes disruption of H-bonding with the pairing base. The bases with disrupted H-bonds are in turn activated toward chlorination and can then form C-chlorinated product(s) that are not reverted to the parent by the reductant (irreversible Cchlorination) (eq 2). The higher the FAC exposure, and the more nucleotide bases that become N-chlorinated (with concomitant disruption of H-bonds), the faster the irreversible C-chlorination becomes, until the monitored amplicon is fully N-chlorinated and the observed rate of amplicon degradation reaches a maximum (consistent with the trends shown in Figures 1, S4, and S6). Further discussions on the complex kinetics of FAC and the determination of $k_{\rm FAC,Amp}$ values are provided in SI-Text-7, SI-Excel-FAC, and He et al. (2019).²⁹ The resulting values of $k_{\rm FAC,Amp}$ (N-chlorination rate constants for each amplicon) were $3.7(\pm0.7) \times 10^3$, $6.2(\pm0.5) \times 10^3$, and $9.9(\pm0.6) \times 10^3$ M⁻¹ s⁻¹ for the 212, 612, and 1018 bp amplicons. $k_{\text{FAC,N-Cl bp}}$, the rate constant for C-chlorination of individual base pairs, was determined to be $2.9(\pm 0.2) \times 10^{-1}$ M^{-1} s⁻¹, from which $k_{FAC,AmpN-Cl}$ could be calculated as $k_{\mathrm{FAC,AmpN-Cl}} = k_{\mathrm{FAC,N-Cl}\,\mathrm{bp}} \times \left(\frac{\mathrm{\#N-Cl}\,\mathrm{bp}}{\mathrm{Amp}_{\mathrm{N-Cl}}}\right), \text{ where } \left(\frac{\mathrm{\#N-Cl}\,\mathrm{bp}}{\mathrm{Amp}_{\mathrm{N-Cl}}}\right)$

the average number of
$$N$$
-chlorinated base pairs in a population of N -chlorinated amplicons (SI-Text-7). The $k_{\rm FAC,Amp}$ and $k_{\rm FAC,N-Cl\ bp}$ values for $mecA$ were in good agreement with those previously reported for chromosomal $B.subtilis$ ARG (blt). ²⁹

The kinetics and rate constants of mecA amplicon degradation by FAC were also determined at pH 8.5 (Figures S7 and S8) and different temperatures (5–30 °C, pH 7, Figures S9 and S10) using the same modeling approach as that described in SI-Text-7. The obtained $k_{\rm FAC,Amp}$ and $k_{\rm FAC,N-Clbp}$ values are summarized in Tables S3 and S4. The $k_{\rm FAC,Amp}$ of pH 8.5 were lower than those of pH 7.0 by a factor of 2–3, which could be due to decreasing proportion of HOCl (typically the more reactive free chlorine species compared to OCl $^-$) with increasing pH. 50 The activation energies for $k_{\rm FAC,Amp}$ were determined to be in the range of 45–48 kJ/mol (Figure S11 and Table S4).

The degradation kinetics of extra-mecA by O_3 are described here (Figures 1b and S5). The degradation of mecA by O₃ (with *OH scavenged by tert-butanol) followed linear kinetics with increasing O₃ exposure, indicating second-order reaction kinetics with respect to mecA and O3. The resulting secondorder rate constants $(k_{\rm O3,Amp})$ were $2.9(\pm 0.4) \times 10^4$, $4.9(\pm 0.3) \times 10^4$, and $6.2(\pm 0.6) \times 10^4$ M⁻¹ s⁻¹ for the 212, 612, and 1018 bp amplicons, respectively, in good agreement with rate constants previously reported for the B. subtilis blt gene.²⁹ The kinetics of mecA amplicon degradation by O3 were also investigated without tert-butanol, and were faster than those in the presence of tert-butanol by a factor of ~ 3 based on the obtained apparent second-order rate constants (Figures S5 vs S12). This finding can be understood as resulting from a contribution of OH to the degradation of DNA during ozonation in which OH is likely formed from the reaction of O₃ with the adenine moiety.^{51,52} Consistent with the result observed for mecA, the second-order rate constant for the reaction of O₃ with calf thymus DNA has been reported to be 1.1×10^3 and 4.1×10^2 M⁻¹ s⁻¹ in the absence and presence of *tert*-butanol, respectively, ⁵¹ showing a similar factor of ~3 difference.

The degradation kinetics of extra-*mecA* by <u>UV</u> are described here (Figures 1c and S13). The degradation of *mecA* amplicons by UV exhibited decelerating (or tailing) kinetics. The decelerating trend in kinetics was particularly notable for the 212 bp amplicon. Similar decelerating kinetics have been reported for extra-ARG degradation by UV in prior studies, ^{20,28,29} with the tailing effect *qualitatively* attributed to the photoreversal of cyclobutane pyrimidine dimers (CPDs). ^{53–55} In this study, photoreversal has been *quantitatively* incorporated into a new kinetic model proposed for the degradation of *mecA* amplicons by UV, comprising formation of CPDs as the predominant UV-induced lesions (eq 3 forward), photoreversal of the CPDs (eq 3 reverse), and parallel, irreversible formation of lesions such as (6–4) photoproducts (64PPs) (eq 4). ^{55,56}

$$Amp + UV \xrightarrow[k_{UV,PR-CPDs,Amp}]{k_{UV,PR-CPDs,Amp}} Amp_{CPD} + UV$$
(3)

$$Amp + UV \xrightarrow{k_{UV,64PPs,Amp}} Amp_{64PP}$$
 (4)

On the basis of eqs 3 and 4, the rate of mecA degradation by UV can be expressed as eq 5 in which $k_{\rm UV,CPDs,Amp}$, $k_{\rm UV,PR-CPDs,Amp}$, and $k_{\rm UV,64PPs,Amp}$ are fluence-based rate constants for eq 3 (forward and reverse) and eq 4, respectively. Among these rate constants, $k_{\rm UV,PR-CPDs,Amp}$ values vary with the extent of CPD formation on the basis of the assumption that only amplicons containing a single CPD (and no 64PPs) can be directly reverted to their undamaged forms (containing

only undamaged parent bipyrimidine doublets), whereas amplicons containing multiple CPDs cannot be directly reverted to their undamaged forms by a single step of photoreversal. Note that each amplicon can sustain multiple CPDs up to a maximum number equal to the number of bipyrimidine doublets of the amplicon. Thus, $k_{\text{UV,PR-CPDs/Amp}}$ can be expressed as a product of a rate constant for photoreversal of a single CPD $(k_{\rm UV,PR-singleCPD})$ and the fraction of amplicons having a single CPD in a population of amplicons with CPDs $(f_{\text{singleCPD}} = [Amp_{\text{singleCPD}}]/[Amp_{\text{CPDs}}])$, as expressed in eq 6. If UV-induced CPD formation follows a Poisson distribution, an average number of CPDs (λ_{CPDs}) can be calculated as $\lambda_{CPDs} = -\ln([Amp]/[Amp]_0)$, and the $f_{singleCPD}$ parameter can be calculated as $f_{\text{singleCPD}} = \lambda_{\text{CPDs}} \times \exp(-\lambda_{\text{CPDs}})$. Further details of these equations based on poisson distribution can be found elsewhere.⁵⁷ Finally, using the relationship $[Amp_{CPDs}] \approx ([Amp]_0 - [Amp])$ (in which a presumably minor population of amplicons having both CPDs and 64PPs is not considered), eq 5 can be rearranged and expressed as eq 7

$$\frac{\text{d[Amp]}}{\text{dt}} = k_{\text{UV,PR-CPDs,Amp}}[\text{Amp}_{\text{CPDs}}] - k_{\text{UV,CPDs,Amp}}[\text{Amp}] - k_{\text{UV,64PPs,Amp}}[\text{Amp}]$$
(5)

$$k_{\text{UV,PR-CPDs,Amp}} = k_{\text{UV,PR-singleCPD}} \times f_{\text{singleCPD}}$$

= $k_{\text{UV,PR-singleCPD}} \times \lambda_{\text{CPDs}} \times e^{-\lambda_{\text{CPDs}}}$ (6)

$$\frac{\text{d[Amp]}}{\text{dt}} = k_{\text{UV,PR-CPDs,Amp}}[\text{Amp}]_0$$

$$- [k_{\text{UV,CPDs,Amp}} + k_{\text{UV,PR-CPDs,Amp}}$$

$$+ k_{\text{UV,64PPs,Amp}}][\text{Amp}]$$
(7)

As a first step for determining the rate constants in eq 7, the $k_{\mathrm{UV,64PPs,Amp}}$ value was determined from the linear slopes of logarithmic plots of 212 bp amplicon degradation at extended UV fluence (>600 mJ/cm²) (Figure S14). The linear region of the degradation curve at extended UV fluences can be interpreted as indicating a condition under which the rates of UV-induced CPD formation and photoreversal become equal, reaching a pseudoequilibrium state, and the formation of 64PPs is solely responsible for the observed degradation of the mecA amplicon. Formation rates of 64PPs are known to be slower than those of CPD formation and photoreversal. 55,58 As the result, a $k_{\rm UV,64PPs,Amp}$ value of $3.2(\pm0.4)\times10^{-3}~{\rm cm^2/mJ}$ was determined for the 212 bp amplicon (Figure S14). The same approach could not be applied to the 612 bp and 1018 bp amplicons because the concentrations of these longer amplicons decreased below the qPCR quantification limits before the degradation curve reached the pseudoequilibrium linear kinetics region (Figure S13). As the thymine-cytosine 64PP (TC-64PP) is the most frequent 64PP, 58 a rate constant specific to a single TC site could be estimated as $k_{\rm UV, single 64PP} = \frac{k_{\rm UV, 64PPs, Amp}}{\#{\rm TC}} = 1.8(\pm 0.2) \times 10^{-4} {\rm cm}^2/{\rm mJ}$ based on an assumption that $k_{\mathrm{UV,64PPs,Amp}}$ is linearly proportional to the number of TC sites of the 212 bp amplicon (#TC = 18, Table S5). The $k_{\rm UV,64PPs,Amp}$ values for the 612 bp and 1018 bp amplicons were then estimated by multiplying $k_{UV,single64PP}$ by the respective number of TC sites for each amplicon (64 and 105, Table S5), assuming that the $k_{UV,single64PP}$ value obtained

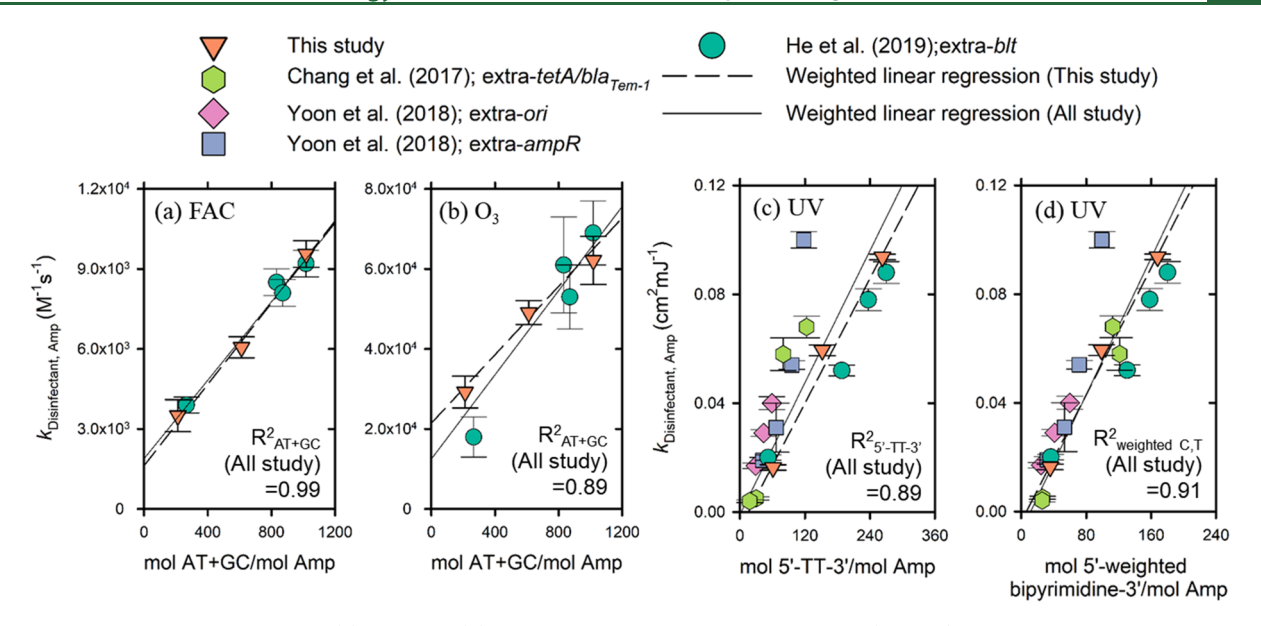


Figure 2. Bimolecular rate constants for (a) FAC and (b) O₃, and fluence-based rate constants for (c and d) UV, plotted versus molar contents of nucleotide base pairs (mol AT+GC/mol Amp) or specific doublets (mol 5'-TT-3'/mol Amp and mol 5'-weighted bipyrimidine-3'/mol Amp) for the 212, 612, and 1018 bps extra-*mecA* amplicons. The rate constants were obtained from kinetic modeling of the data shown in Figure 1, following the methods described in the main text. Error bars represent standard errors from kinetic model fitting (Table S3). Rate constants reported for extracellular DNA at pH 7 from the literature are shown for comparison and taken from Yoon et al. (2018),²⁷ He et al. (2019),²⁹ and Chang et al. (2017).²⁸ Lines represent the weighted linear regressions for the rate constants from this study alone (dashed lines) and from both this study and literature data (solid lines).

from the 212 bp amplicon represents an average value applicable to all three *mecA* amplicons.

Following determination of the rate constants for the formation of 64PPs, the $k_{\rm UV,CPDs,Amp}$ and $k_{\rm UV,PR-singleCPD}$ values could be determined for each amplicon by fitting of the experimental data (ln([Amp]/[Amp₀]) vs UV fluence) with model predictions based on eqs 5-7, which were performed using the same numerical approach as that for the FAC model (SI-Excel-UV). The resulting $k_{\rm UV,CPDs,Amp}$ values were $2.0(\pm 0.1) \times 10^{-2}$, $4.8(\pm 0.3) \times 10^{-2}$, and $7.6(\pm 0.5) \times 10^{-2}$ cm²/mJ for the 212, 612, and 1018 bp amplicons, respectively (similar to apparent rate constants previously obtained for the B. subtilis blt gene by assuming the ARG degradation followed simple linear kinetics at low fluences, without explicitly accounting for CPD reversal or 64PP formation),²⁹ and the resulting $k_{\rm UV,PR-singleCPD}$ value was $4.9(\pm 0.5) \times 10^{-3}~{\rm cm^2/mJ}$. Note that for the kinetic parameter for CPD photoreversal, $k_{\text{UV,PR-singleCPD}}$ could be determined as a time-<u>in</u>dependent rate constant, whereas $k_{\text{UV,PR-CPDs,Amp}}$ is a time-dependent rate constant that must be calculated using the $k_{\rm UV,PR\text{-}singleCPD}$ value and eq 6. Overall, our new kinetic model for the UV photolysis of DNA successfully simulates the degradation of mecA, inclusive of the observed tailing kinetics (see the lines in Figures 1c and S13).

Effect of Amplicon Length and Nucleotide Content on Degradation Rate of Extra-mecA. For FAC and O_3 , the $k_{\text{FAC,Amp}}$ and $k_{\text{O3,Amp}}$ values were found to increase linearly with increasing mecA amplicon length, expressed as (mol AT+GC)/(mol Amp) (Figure 2a,b), consistent with trends reported previously for the *B. subtilis blt* gene. This observation reflects the fact that the number of potential sites of reaction with these disinfectants increases with increasing amplicon length and that FAC and O_3 are expected to react with both GC and AT base pairs in double-stranded DNA, as inferred from the high reactivity of each of these disinfectants toward guanine

(G) and thymine (T) nucleotides. ^{51,59} The $k_{\rm FAC,Amp}$ and $k_{\rm O3,Amp}$ values of this study were fitted to eq 8 by means of uncertainty-weighted linear regression using Excel spreadsheets (SI-Excel-Reg) as previously described. ²⁹ Weighted linear regressions were used since these rate constants themselves carry associated standard errors. In eq 8, $k_{\rm Disinfectant,X}$ as the slope represents the rate constant normalized to molar content of X per amplicon (where X is AT+GC bps for FAC and O₃, or 5'-TT-3' doublets for UV), and $k_{\rm Disinfectant,0}$ is the intercept of linear regression.

$$k_{\text{Disinfectant,Amp}} = k_{\text{Disinfectant,X}} \times \frac{\text{mol}_{X}}{\text{mol}_{\text{Amp}}} + k_{\text{Disinfectant,0}}$$
(8)

For FAC, a $k_{\rm FAC,AT+GC}$ value of 7.6(±0.5) (M AT+GC)⁻¹s⁻¹ and a $k_{\rm FAC,0}$ value of 1.6(±0.4) × 10³ M⁻¹ s⁻¹ were obtained, which are close to those reported previously for the B. subtilis blt gene $(k_{\text{FAC,AT+GC}} = 7.2(\pm 0.5) \text{ (M AT+GC)}^{-1} \text{s}^{-1} \text{ and } k_{\text{FAC,0}} = 2.1(\pm 0.4) \times 10^3 \text{ M}^{-1} \text{ s}^{-1}).^{29} \text{ These } k_{\text{FAC,AT+GC}} \text{ values are}$ somewhat lower but also still comparable to the rate constant for the reaction of FAC with DNA (\sim 20 (M AT+GC)⁻¹s⁻¹) reported by Prütz based on denaturation of dsDNA.⁵⁹ The relatively large positive value for $k_{\rm FAC,0}$ (relative to the magnitude of $k_{FAC,AT+GC}$) has been attributed to factors affecting DNA reactivity that are not captured in the simple single-parameter model represented by eq 8, such as the presence of specific nucleotide sequences showing especially high susceptibility to oxidation (e.g., guanine or thymine multiplets). ^{29,60} For O₃, a $k_{\text{O3,AT+GC}}$ value of $4.3(\pm 0.5) \times 10^{1}$ $(M \text{ AT+GC})^{-1} \text{s}^{-1}$ and a $k_{03,0}$ value of $2.1(\pm 0.3) \times 10^4 \text{ M}^{-1}$ $m s^{-1}$ were obtained. Compared with the values of $k_{
m O3,AT+GC}$ and $k_{\rm O3,0}$ reported previously for the *B. subtilis blt* gene (6.5(±0.7) \times 10¹ (M AT+GC)⁻¹s⁻¹ and 0.5(±4.5) \times 10³ M⁻¹ s⁻¹, respectively), ²⁹ the value of $k_{O3,AT+GC}$ in this study was in relatively good agreement (~1.5-fold lower) though the value

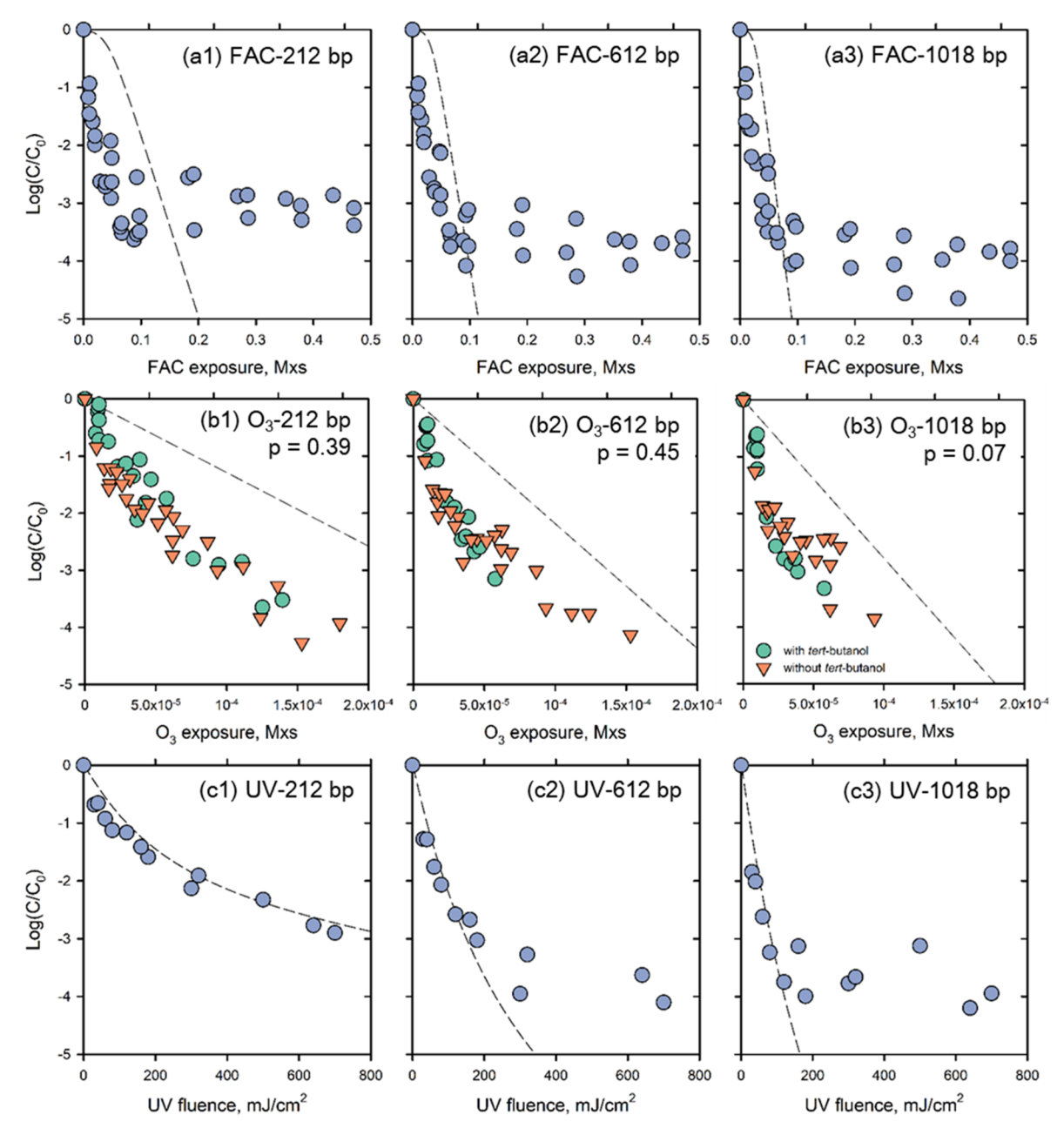


Figure 3. Logarithmic relative concentration of intra-*mecA* 1018 bp qPCR amplicons as a function of disinfectant exposure or UV fluence during treatment of MRSA BAA-1556 at pH 7 (10 mM phosphate buffer) with (a) FAC, (b) O₃, and (c) UV. The O₃ treatments were performed in the absence and presence of *tert*-butanol (50 mM). Statistical significance of differences in data obtained in the absence versus presence of *tert*-butanol was examined by paired *t*-test using Prism 6 (GraphPad). Up to 5-log decrease in intra-*mecA* concentrations could be quantified by the qPCR method in the tested experimental conditions. Symbols are the measured data, and dotted lines represent predicted kinetics of extra-*mecA* degradation generated by fitting the data of current work (Figure 1, shown for comparison).

of $k_{\rm O3,0}$ was ~40-fold higher. With consideration of the limited number of reported values thus far available to develop these correlations, more data are needed to further test the broader applicability of the single-parameter model (eq 8) to other ARGs and/or other forms of DNA (e.g., plasmid-borne ARGs). The $k_{\rm O3,AT+GC}$ value from this study was lower than the rate constant for the reaction of O₃ with calf thymus DNA (8.2 × 10^2 (M AT+GC) $^{-1}$ s $^{-1}$) reported by Theruvathu et al. in which the rate constant was determined by measuring O₃ decomposition in the presence of excess DNA. The different $k_{\rm O3,AT+GC}$ values might be attributable to the differences in the analytical and kinetic methods used in this study and the prior study, 51 which warrants further investigation.

For UV, the sums of $k_{\rm UV,CPDs,Amp}$ and $k_{\rm UV,64PPs,Amp}$ values (i.e., $k_{\rm UV,Amp}=k_{\rm UV,CPDs,Amp}+k_{\rm UV,64PPs,Amp})$ were used here for the correlation/comparison analyses because the DNA degradation rate constants available from the literature were measured as composite parameters without separating the contributions from CPD and 64PP formation. It should be noted, nevertheless, that CPD formation was the dominant (~86%) contributor to the overall UV-induced DNA degradation $(k_{\rm UV,CPDs,Amp}\approx 6.1\times k_{\rm UV,64PPs,Amp})$ based on our kinetic model. The $k_{\rm UV,Amp}$ values increased linearly with the number of intrastrand thymine doublets per amplicon (mol 5′-TT-3′/mol Amp), consistent with the understanding of 5′-TT-3′ as one of the most photoreactive bipyrimidine sites (Figure 2c). 53 From

the weighted linear regression based on eq 8, a $k_{UV,TT}$ value of $3.8(\pm 0.2) \times 10^{-4} \text{ (M 5'-TT-3'/M amplicon)}^{-1} \text{ (cm}^2/\text{mJ)}$ and a $k_{\rm UV,0}$ value of $-6.0(\pm 3.6) \times 10^{-3} \ {\rm cm^2/mJ}$ were obtained, which are close to those from literature $(k_{\rm UV,TT} = 4.0(\pm 1.7) \times$ 10^{-4} (M 5'-TT-3'/M amplicon)⁻¹(cm²/mJ) and $k_{\rm UV,0} = -1.0(\pm 9.4) \times 10^{-3}$ M⁻¹ s⁻¹). $^{26,28-30}$ The $k_{\rm UV,Amp}$ data were also correlated with the sum of molar light absorption and quantum yield-weighted numbers of each of the four possible bipyrimidine sites 5'-TT-3', 5'-TC-3', 5'-CT-3', and 5'-CC-3' (Figure 2d). This is based on the expectation that the bipyrimidines other than TT doublets (i.e., TC, CT and CC doublets) also contribute to the overall CPD formation rate, but with different photoreactivities.⁵⁸ The relative contributions of each bipyrimidine site to the overall lesion formation can be estimated as 0.40, 0.49, 0.082, and 0.026 for TT, TC, CT, and CC doublets, respectively (derived by multiplying respective molar light absorption coefficients and quantum yield values for TT, TC, CT, and CC doublets, Table S7).^{29,42} The weighted numbers of each bipyrimidine were then calculated as mol weighted 5'-bipyrimidine-3'/mol Amp = $(0.40 \times (\text{mol } 5'-\text{TT}-3')+0.49 \times (\text{mol } 5'-\text{TC}-3')+0.082 \times (\text{mol } 5'-\text{TC}-3')$ 5'-CT-3')+0.026 × (mol 5'-CC-3'))/mol Amp as described in He et al. (in preparation).⁴² A better linear correlation was obtained ($R^2 = 0.91$, Figure 2d) when the weighted numbers of all bipyrimidines were used than when using only the number of 5'-TT-3' sites (R²=0.89, Figure 2c). A $k_{UV,weighted bipyrimidines}$ value of $5.8(\pm 0.2) \times 10^{-4}$ (M weighted bipyrimidine/M amplicon)⁻¹(cm²/mJ) and a $k_{\rm UV,0}$ value of $-3.7(\pm 2.6) \times 10^{-3}$ cm²/mJ were obtained, which are close to those obtained by performing regression of the data from prior studies^{26,28–36} (i.e., $k_{\rm UV, weighted\ bipyrimidines} = 6.3(\pm 2.5) \times 10^{-4}$ (M weighted bipyrimidine/M amplicon)⁻¹(cm²/mJ) and $k_{\rm UV,0} =$ $-0.73(\pm 1.1) \times 10^{-2}$ cm²/mJ). Correlations of fluence-based rate constants for degradation of chromosomal DNA by UV versus number of 5'-TT-3' doublets or weighted number of total 5'-bipyrimidine-3' sites are more scattered than in the cases of FAC and O3 due to the combination of wider variability in $k_{\mathrm{UV,Amp}}$ values reported here and in the literature and variations in the kinetics models used for rate constant determination between different studies. In addition, such differences could be caused by variability in photoreactivities of bipyrimidines depending on their neighboring nucleotides, 55 which has not been captured in the kinetic model presented here or in most prior work.

Good overall linear correlations have also been found here for values of $k_{\rm FAC,Amp}$, $k_{\rm O3,Amp}$ and $k_{\rm UV,Amp}$ versus amplicon length or bipyrimidine contents when combining the data from this study and from previous literature (solid line, Figure 2), inclusive of findings for both chromosomal and plasmid DNA for UV. $^{26,28-30}$ The latter observation indicates a relatively minor effect of DNA conformation on the DNA reactivity toward UV. The resulting $k_{\rm Disinfectant,X}$ and $k_{\rm Disinfectant,0}$ values when using the available data from all studies are summarized in Table S3.

Kinetics of MRSA Inactivation and Cellular Component Damage. Figure S15 shows concentration changes for culturability (plate counting), membrane damage (FCM-ICC), and severe DNA damage (e.g., DNA fragmentation) (FCM-TCC) as a function of disinfectant exposure or UV fluence during treatment of MRSA with (a) FAC, (b) O_3 , and (c) UV at pH 7. The FCM-TCC and ICC data are shown in SI Figures FCM1-FCM6 and discussed in SI-Text-8. For FAC and O_3 , loss of culturability occurred first $(k_{\rm FAC}$ of $1.6(\pm 0.1) \times 10^5$

 $M^{-1} s^{-1}$ and k_{O3} of >4 × 10⁵ $M^{-1} s^{-1}$), followed by damage to the cell membrane $(k_{\rm FAC} \text{ of } 8.3(\pm 0.3) \times 10^4 \text{ M}^{-1} \text{ s}^{-1} \text{ and } k_{\rm O3}$ of $1.6(\pm 0.1) \times 10^5 \text{ M}^{-1} \text{ s}^{-1}$), and then followed by severe DNA damage, where the parentheses show the second-order rate constants determined for culturability loss and cell membrane damage from the slopes of the linear plots in Figure S15 (note that severe DNA damage kinetics were complex and could not be described by a single k value for either FAC or O₃).⁶¹ Note that more than a 5-log reduction in the culturable cell concentration was observed for O3 at the lowest O_3 exposure (= 3.3×10^{-5} M \times s). For UV, loss of culturability was efficient ($k_{\rm UV}$ of $4.2(\pm 0.3) \times 10^{-1} {\rm cm}^2/{\rm mJ}$), but cell membrane damage and severe DNA damage were negligible. The observed sequences of events are consistent with the known bactericidal modes of action of these disinfectants.⁶² FAC and O₃, as chemical agents, first attack outer cellular components (i.e., membrane) and then diffuse into the cell causing degradation of intracellular components such as DNA.⁶³ UV directly interacts with DNA as a physical agent causing DNA base modification (e.g., CPD or 64PP formation) but does not induce structural degradation of DNA or membrane damage at typical germicidal fluences. 13,63 The rate constants of inactivation/damage observed for MRSA by each disinfectant were comparable to those of laboratorycultured E. coli but much higher than those of autochthonous bacteria in natural water or wastewaters. 27,48,64 Overall, substantial levels of severe DNA damage resulted from treatment with FAC and O3 under the investigated conditions (i.e., > 1-log decrease at an exposure of 9.0×10^{-2} M \times s for FAC and 5×10^{-5} M × s for O_3) but not from UV treatment.

Degradation Kinetics of Intra-mecA and Its Comparison to Extra-mecA. Figure 3 shows the logarithmic relative concentration of the intra-mecA 212, 612, and 1018 bp qPCR amplicons as a function of disinfectant exposure or UV fluence during treatment of MRSA at pH 7 with (a) FAC, (b) O₃, and (c) UV. The ozonation experiments were performed in the absence and presence of *tert*-butanol (50 mM). Levels of *mecA* degradation during FAC and O₃ treatments were dependent on oxidant exposures but were independent of initial FAC (Figure S16) or O₃ concentrations (Figure S17) used to achieve a given oxidant exposure. The dotted lines in Figure 3 show degradation kinetics of extra-mecA under the same conditions (Figure 1) for comparison.

The following trends were notable for the degradation kinetics of intra-mecA. In the case of FAC (Figure 3a), the intra-mecA showed faster degradation than the extra-mecA at low FAC exposure ($<0.1 \text{ M} \times \text{s}$), but its degradation became slow and nearly ceased at 3-4 logs of loss as the FAC exposure increased from 0.1 to 0.5 M \times s. The initial more rapid degradation of intra-mecA than extra-mecA was also observed for O₃ (with and without tert-butanol; Figure 3b). With increasing O₃ exposure, the degradation rate of intra-mecA decreased and became similar to that of extra-mecA. The degradation of intra-mecA by O₃ did not show significant tailing kinetics at higher exposures, as those observed for FAC and UV, and continued with increasing O3 exposure. The intra-mecA degradation kinetics during treatment with O₃ were not significantly different in the absence and presence of tertbutanol (p = 0.07-0.45), indicating negligible influence of extracellularly produced *OH on the intra-*mecA* degradation, consistent with prior observations. ^{22,25,29} In the case of UV, the degradation rate of intra-mecA for the 212 bp amplicon was similar to that of extra-mecA at degradation levels of less than

Increasing FAC exposure

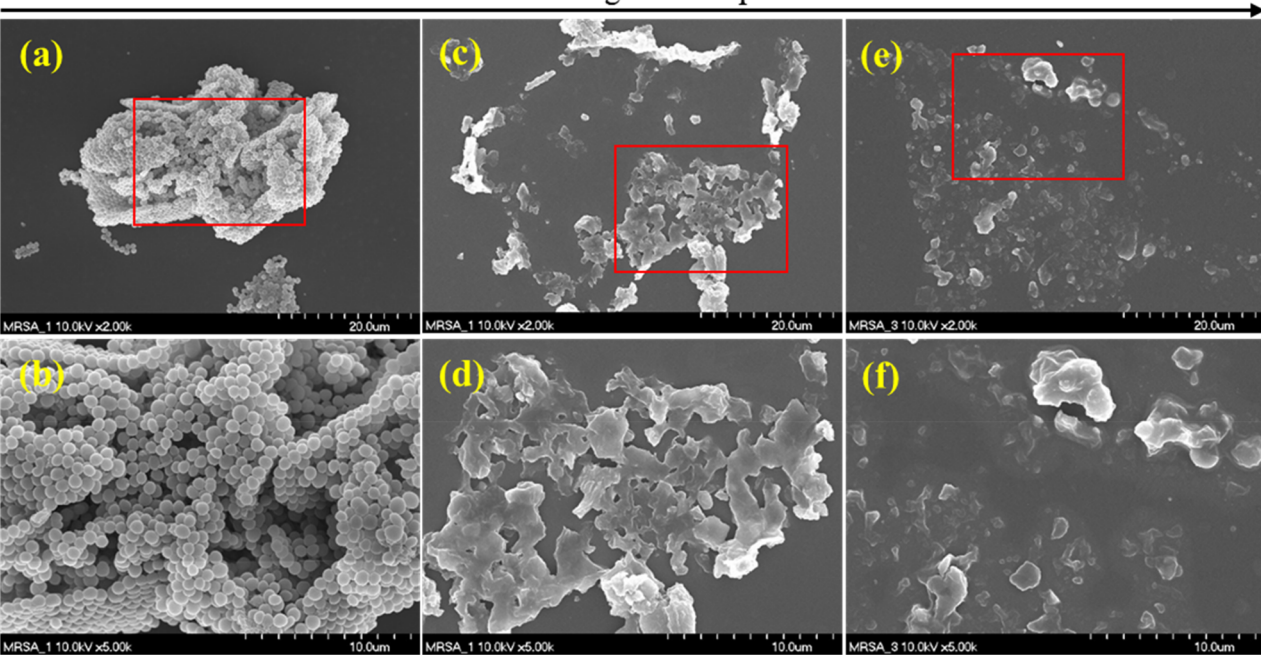


Figure 4. Scanning electron microscopy (SEM) images of MRSA samples (a, b) before and (c-f) after FAC treatment at pH 7. MRSA cells were prepared from a midexponential culture of BAA-1556. The FAC exposure was 0 for parts a and b, 100 for parts c and d, and 500 (mg/L as Cl_2) × min for parts e and f. Parts b, d, and f depict magnified images of the red square areas shown in parts a, c, and e, respectively. Additional SEM images are presented in the SI Figure SEM.

3-logs (Figure 3 c1), but for the 612 bp and 1018 bp amplicons, it slowed and approached zero at the level of ~4logs of loss with increasing UV fluence to 750 mJ/cm² (Figures 3 c2,c3). The initially more rapid decrease observed for intramecA concentration in comparison to extra-mecA for FAC and O₃ is notable, as the opposite result is anticipated considering the expected consumption of FAC or O₃ by cellular constituents. For FAC, the initial intra-mecA degradation rates, which were fitted to a two-phase model, 61 did not show significant statistical differences for amplicons with variable lengths (p = 0.62, Figure S18a). The initial rapid loss of intramecA during FAC treatment is therefore not likely to be caused by any DNA degradation process, because in such a scenario, the intra-mecA loss rate would be expected to increase with amplicon length. A possible cause for this phenomenon during chlorination was variation in DNA recovery efficiency from intact vs chlorinated cells.

To test the preceding hypothesis, MRSA cells were treated with FAC at different FAC exposures, and the samples before and after chlorination were analyzed for both total dsDNA recovery and intra-mecA concentrations. Two different DNA extraction methods were applied, using either the FastDNA spin kit or the PCI method, and the concentration of extracted dsDNA was determined by a fluorescence-based DNA quantification kit (SI-Text-9). The results showed that dsDNA recovery efficiencies from MRSA cells dropped by a factor of ~4 at the FAC exposure of 0.02 M × s in comparison to untreated MRSA cells but did not decrease further with increasing FAC exposure to 0.18 M \times s (Figure S19). Notably, FCM-TCC levels were stable within the FAC exposure range of up to 0.03 M × s (Figure S15), indicating that decreased dsDNA recovery efficiency was not attributable to DNA damage (e.g., strand breakage). Even though the PCI method yielded higher total dsDNA recoveries than the FastDNA spin

kit (Figure S19a), the drop in dsDNA recovery upon chlorination was similar for the two methods (Figure S19b). Following correction for dsDNA recoveries, intra-*mecA* concentration profiles aligned more closely with those observed for extra-*mecA* up to ~0.05 M × s (Figure S20). These results appear to confirm that decreases in DNA recovery from damaged MRSA cells were responsible for the apparent rapid initial decreases of intra-*mecA* concentrations observed following treatment with FAC. One potential reason for the decreased recoveries could be hindrance of DNA separation from proteins due to formation of DNA–protein cross-links upon exposure of MRSA cells to FAC. Further investigation is needed to better understand the lowered DNA recovery from chlorinated cells.

For O_3 , the initial rates of intra-*mecA* loss, which were also fitted to a two-phase model, ⁶¹ increased for the longer amplicons (p = 0.01, Figure S18b), indicating that there may be other cause(s) besides DNA recovery variations (as was observed for FAC). The phenomenon for O_3 could possibly be attributable to a Fenton-like reaction within the bacterial cells initiated by reactions of O_3 with intracellular redox-active iron species that could generate ferryl ions or free radicals and cause oxidative DNA damage. ^{66,67} It is notable that a Fenton-like reaction mechanism has originally been proposed to explain the oxidative DNA damage of *E. coli* induced by exogenous H_2O_2 .

The tailing kinetics were observed at high FAC exposures and UV fluences at which the intra-*mecA* concentrations were nearly all above the qPCR quantification limit. The tailing observed for UV could not be explained solely by photoreversal of CPDs, since it was much more significant than that accounted for by the photoreversal model. One potential explanation for the excess tailing could be the formation of MRSA aggregates, the interior of which may have protected

intracellular DNA from FAC and UV. $^{69-71}$ A potential role of aggregates could be supported by SEM images in which aggregates of sizes in excess of 30 μm in length and consisting of large numbers of cells were observed (Figure 4 and SI Figure SEM). The SEM images of chlorinated MRSA samples (FAC exposures of 100 and 500 (mg/L as Cl₂) × min) showed that parts of these aggregates were destroyed or disintegrated but that the aggregate structures were still maintained (Figures 4c–f). The UV treatment did not appear to affect aggregation (SI Figure SEM).

In additional experiments, MRSA suspensions were pretreated by sonication to disrupt the aggregates and then treated by FAC at pH 7 (in which case the sonication itself was confirmed in controls not to yield any direct membrane damage which might affect mecA degradation). Sonicated MRSA samples showed less tailing in kinetics of intra-mecA degradation (for 612 and 1018bp amplicons) by FAC than the control samples without sonication (Figure S21) (p < 0.01). This indicates that disruption of the aggregates by sonication partially abolished the protection of intra-mecA against FAC. It is less clear whether such aggregates are relevant for MRSA in municipal wastewaters. Nonetheless, our results highlight the potential importance of cell aggregates or cells attached to or embedded in particles in hindering degradation of intracellular-ARGs by disinfectants, similar to detrimental effects of aggregation observed in relation to inactivation of bacterial cells themselves. 70,72

Implications for Predicting and Controlling the Degradation and Deactivation of ARGs. It has been demonstrated here that the degradation kinetics of extra-mecA during exposure to FAC, O3, and UV can be well described and predicted by the kinetic models developed in this study (UV) and in prior work (FAC and O₃)²⁹ in combination with the updated rate constant information summarized in Table S3. This also supports the finding that kinetics-based models can enable a generalized prediction of the disinfectant-induced degradation of ARGs including (if known) critical sequences required for the ARGs' HGT (e.g., by natural transformation).²⁹ However, deviations in the kinetics observed for degradation of extra-mecA versus degradation of intra-mecA in MRSA cells (e.g., tailing in intra-mecA losses due to MRSA aggregates and apparent rapid drops in intra-mecA concentrations due to decreased DNA recovery from oxidized cells) signify a need for further study and caution in assessing and predicting the efficiencies of intracellular ARG degradation during water disinfection.

SCCmec has been found in different staphylococcal strains and species, indicating that this mobile genetic element is transferrable among staphylococci. The Under laboratory conditions, the transfer of SCCmec has been demonstrated to occur via all three HGT mechanisms (i.e., conjugation, transduction including autotransduction, transformation autotransduction, though the significance of each potential SCCmec transfer pathway for mechanisms dissemination in real environments remains unclear. With the assumption that the mechanism gene must be fully intact to undergo successful HGT by any of these mechanisms, qPCR measurements of mechanisms damage by FAC, UV, or O₃ can provide a conservative indication of each disinfectant's potential to eliminate the possibility of mechanisms (waste) water treatment. Accordingly, the >3-log₁₀ losses of extra-mechanisms and lov treatment at exposures and/or fluences typical of

(waste)water disinfection indicate that each process is capable of mitigating the potential for *mecA* HGT under practical conditions. Furthermore, it was also shown that each of the three disinfectants can efficiently inactivate MRSA (by more than 5-log₁₀) at typical (waste)water disinfection conditions. This provides additional evidence that FAC, O₃, and UV can mitigate *mecA* mobilization via conjugation (as this HGT pathway requires viable donor cells).

ASSOCIATED CONTENT

Supporting Information

The Supporting Information is available free of charge at https://pubs.acs.org/doi/10.1021/acs.est.0c05274.

Details of DNA extraction, analytical methods and results (including CFU, FCM, qPCR, and SEM), and disinfection experiments; ARG and primer sequences and nucleotide contents; degradation kinetics of extra-and intra-*mecA* by each disinfectant; detailed discussions of FAC and UV reaction kinetics, mechanisms, and associated kinetic model development; MRSA inactivation, membrane and DNA damage; Effect of FAC treatment on DNA recovery efficiency (SI-Word) (PDF)

Kinetic model fittings for FAC and UV reactions (SI-Excel-FAC, SI-Excel-UV); weighted linear regressions of $k_{\rm Disinfectant,\ Amp}$ versus molar contents of various nucleotide bps, TT-doublets, and weighted bipyrimidine doublets (SI-Excel-Reg) (ZIP)

AUTHOR INFORMATION

Corresponding Author

Yunho Lee — School of Earth Sciences and Environmental Engineering, Gwangju Institute of Science and Technology (GIST), Gwangju 61005, Republic of Korea; oocid.org/0000-0001-5923-4897; Phone: 82-62-715-2468; Email: yhlee42@gist.ac.kr; Fax: 82-62-715-2434

Authors

Yegyun Choi — School of Earth Sciences and Environmental Engineering, Gwangju Institute of Science and Technology (GIST), Gwangju 61005, Republic of Korea; ⊙ orcid.org/0000-0003-2177-1181

Huan He − Department of Civil and Environmental Engineering, University of Washington (UW), Seattle, Washington 98195-2700, United States; ocid.org/0000-0002-0550-0974

Michael C. Dodd — Department of Civil and Environmental Engineering, University of Washington (UW), Seattle, Washington 98195-2700, United States; orcid.org/0000-0001-7544-1642

Complete contact information is available at: https://pubs.acs.org/10.1021/acs.est.0c05274

Notes

I

The authors declare no competing financial interest.

■ ACKNOWLEDGMENTS

This study was supported by National Research Foundation of Korea funded by the Ministry of Science, ICT and Future Planning (NRF- 2020R1A2C2011951). Additional support for Huan He and Michael C Dodd from U.S. National Science Foundation Grant Number CBET-1254929 and the Allan &

Inger Osberg Endowed Professorship is gratefully acknowledged.

REFERENCES

- (1) CDC Antibiotic Resistance Theats in the United States, 2013; U.S. Department of Health and Human Services Centers for Disease Control and Prevention: 2013.
- (2) WHO, No Time To Wait: Securing the future from drugresistant infections. In Report to the Secretary-General of the United Nations 2019.
- (3) Davies, J.; Davies, D. Origins and Evolution of Antibiotic Resistance. *Microbiol. Mol. Biol. Rev.* **2010**, 74 (3), 417–433.
- (4) Thomas, C. M.; Nielsen, K. M. Mechanisms of, and Barriers to, Horizontal Gene Transfer between Bacteria. *Nat. Rev. Microbiol.* **2005**, 3 (9), 711–721.
- (5) Pruden, A.; Pei, R. T.; Storteboom, H.; Carlson, K. H. Antibiotic resistance genes as emerging contaminants: Studies in northern Colorado. *Environ. Sci. Technol.* **2006**, *40* (23), 7445–7450.
- (6) Czekalski, N.; Berthold, T.; Caucci, S.; Egli, A.; Bürgmann, H. Increased levels of multiresistant bacteria and resistance genes after wastewater treatment and their dissemination into Lake Geneva, Switzerland. *Front. Microbiol.* **2012**, *3* (106), 1–18.
- (7) Luo, Y.; Yang, F.; Mathieu, J.; Mao, D.; Wang, Q.; Alvarez, P. J. J. Proliferation of Multidrug-Resistant New Delhi Metallo- β -lactamase Genes in Municipal Wastewater Treatment Plants in Northern China. *Environ. Sci. Technol. Lett.* **2014**, 1 (1), 26-30.
- (8) Xi, C. W.; Zhang, Y. L.; Marrs, C. F.; Ye, W.; Simon, C.; Foxman, B.; Nriagu, J. Prevalence of Antibiotic Resistance in Drinking Water Treatment and Distribution Systems. *Appl. Environ. Microbiol.* **2009**, 75 (17), 5714–5718.
- (9) Berendonk, T. U.; Manaia, C. M.; Merlin, C.; Fatta-Kassinos, D.; Cytryn, E.; Walsh, F.; Bürgmann, H.; Sørum, H.; Norström, M.; Pons, M.-N. Tackling antibiotic resistance: the environmental framework. *Nat. Rev. Microbiol.* **2015**, *13* (5), 310.
- (10) Pruden, A. Balancing Water Sustainability and Public Health Goals in the Face of Growing Concerns about Antibiotic Resistance. *Environ. Sci. Technol.* **2014**, *48* (1), 5–14.
- (11) Jacangelo, J. G.; Trussell, R. R. International report: water and wastewater disinfection trends, issues and practices. *Water Sci. Technol.: Water Supply* **2002**, *2* (3), 147–157.
- (12) von Gunten, U. Oxidation Processes in Water Treatment: Are We on Track? Environ. Sci. Technol. 2018, 52 (9), 5062-5075.
- (13) Dodd, M. C. Potential impacts of disinfection processes on elimination and deactivation of antibiotic resistance genes during water and wastewater treatment. *J. Environ. Monit.* **2012**, *14*, 1754–1771.
- (14) Rizzo, L.; Manaia, C.; Merlin, C.; Schwartz, T.; Dagot, C.; Ploy, M.; Michael, I.; Fatta-Kassinos, D. Urban wastewater treatment plants as hotspots for antibiotic resistant bacteria and genes spread into the environment: a review. *Sci. Total Environ.* **2013**, 447, 345–360.
- (15) Bouki, C.; Venieri, D.; Diamadopoulos, E. Detection and fate of antibiotic resistant bacteria in wastewater treatment plants: a review. *Ecotoxicol. Environ. Saf.* **2013**, *91*, 1–9.
- (16) Lüddeke, F.; Heß, S.; Gallert, C.; Winter, J.; Güde, H.; Löffler, H. Removal of total and antibiotic resistant bacteria in advanced wastewater treatment by ozonation in combination with different filtering techniques. *Water Res.* **2015**, *69*, 243–251.
- (17) Alexander, J.; Knopp, G.; Dötsch, A.; Wieland, A.; Schwartz, T. Ozone treatment of conditioned wastewater selects antibiotic resistance genes, opportunistic bacteria, and induce strong population shifts. *Sci. Total Environ.* **2016**, *559*, 103–112.
- (18) Lin, W.; Zhang, M.; Zhang, S.; Yu, X. Can chlorination coselect antibiotic-resistance genes? *Chemosphere* **2016**, *156*, 412–419.
- (19) Jia, S.; Shi, P.; Hu, Q.; Li, B.; Zhang, T.; Zhang, X.-X. Bacterial Community Shift Drives Antibiotic Resistance Promotion during Drinking Water Chlorination. *Environ. Sci. Technol.* **2015**, 49 (20), 12271–12279.
- (20) McKinney, C. W.; Pruden, A. Ultraviolet disinfection of antibiotic resistant bacteria and their antibiotic resistance genes in

- water and wastewater. Environ. Sci. Technol. 2012, 46 (24), 13393-13400.
- (21) Chen, H.; Zhang, M. Effects of Advanced Treatment Systems on the Removal of Antibiotic Resistance Genes in Wastewater Treatment Plants from Hangzhou, China. *Environ. Sci. Technol.* **2013**, 47 (15), 8157–8163.
- (22) Pak, G.; Salcedo, D. E.; Lee, H.; Oh, J.; Maeng, S. K.; Song, K. G.; Hong, S. W.; Kim, H.-C.; Chandran, K.; Kim, S. Comparison of antibiotic resistance removal efficiencies using ozone disinfection under different pH and suspended solids and humic substance concentrations. *Environ. Sci. Technol.* **2016**, *50* (14), 7590–7600.
- (23) Jäger, T.; Hembach, N.; Elpers, C.; Wieland, A.; Alexander, J.; Hiller, C.; Krauter, G.; Schwartz, T. Reduction of Antibiotic Resistant Bacteria During Conventional and Advanced Wastewater Treatment, and the Disseminated Loads Released to the Environment. *Front. Microbiol.* **2018**, *9*, 2599.
- (24) Zhang, M.; Chen, S.; Yu, X.; Vikesland, P.; Pruden, A. Degradation of extracellular genomic, plasmid DNA and specific antibiotic resistance genes by chlorination. *Front. Environ. Sci. Eng.* **2019**, *13* (3), 38.
- (25) Yoon, Y.; Dodd, M. C.; Lee, Y. Elimination of transforming activity and gene degradation during UV and UV/H 2 O 2 treatment of plasmid-encoded antibiotic resistance genes. *Environmental Science: Water Research & Technology* **2018**, 4 (9), 1239–1251.
- (26) Czekalski, N.; Imminger, S.; Salhi, E.; Veljkovic, M.; Kleffel, K.; Drissner, D.; Hammes, F.; Bürgmann, H.; Von Gunten, U. Inactivation of antibiotic resistant bacteria and resistance genes by ozone: from laboratory experiments to full-scale wastewater treatment. *Environ. Sci. Technol.* **2016**, *50* (21), 11862–11871.
- (27) Yoon, Y.; Chung, H. J.; Di, D. Y. W.; Dodd, M. C.; Hur, H.-G.; Lee, Y. Inactivation efficiency of plasmid-encoded antibiotic resistance genes during water treatment with chlorine, UV, and UV/H2O2. *Water Res.* **2017**, *123*, 783–793.
- (28) Chang, P. H.; Juhrend, B.; Olson, T. M.; Marrs, C. F.; Wigginton, K. R. Degradation of extracellular antibiotic resistance genes with UV254 treatment. *Environ. Sci. Technol.* **2017**, *51* (11), 6185–6192.
- (29) He, H.; Zhou, P.; Shimabuku, K. K.; Fang, X.; Li, S.; Lee, Y.; Dodd, M. C. Degradation and Deactivation of Bacterial Antibiotic Resistance Genes during Exposure to Free Chlorine, Monochloramine, Chlorine Dioxide, Ozone, Ultraviolet Light, and Hydroxyl Radical. *Environ. Sci. Technol.* **2019**, *53* (4), 2013–2026.
- (30) Goldstein, R. E. R.; Micallef, S. A.; Gibbs, S. G.; Davis, J. A.; He, X.; George, A.; Kleinfelter, L. M.; Schreiber, N. A.; Mukherjee, S.; Sapkota, A.; Joseph, S. W.; Sapkota, A. R. Methicillin-Resistant Staphylococcus aureus (MRSA) Detected at Four U.S. Wastewater Treatment Plants. *Environ. Health Perspect.* **2012**, *120* (11), 1551–1558.
- (31) Wan, M. T.; Chou, C. C. Spreading of β -lactam resistance gene (mecA) and methicillin-resistant Staphylococcus aureus through municipal and swine slaughterhouse wastewaters. *Water Res.* **2014**, 64, 288–295.
- (32) Boopathy, R. Presence of Methicillin Resistant Staphylococcus aureus (MRSA) in sewage treatment plant. *Bioresour. Technol.* **2017**, 240. 144–148.
- (33) Amirsoleimani, A.; Brion, G. M.; Diene, S. M.; François, P.; Richard, E. M. Prevalence and characterization of Staphylococcus aureus in wastewater treatment plants by whole genomic sequencing. *Water Res.* **2019**, *158*, 193–202.
- (34) Peacock, S. J.; Paterson, G. K. Mechanisms of methicillin resistance in Staphylococcus aureus. *Annu. Rev. Biochem.* **2015**, *84*, 577–601.
- (35) Haaber, J.; Penadés, J. R.; Ingmer, H. Transfer of antibiotic resistance in Staphylococcus aureus. *Trends Microbiol.* **2017**, *25* (11), 893–905.
- (36) Miragaia, M. Factors contributing to the evolution of Mecamediated β -lactam resistance in staphylococci: update and new insights from whole genome sequencing (WGS). *Front. Microbiol.* **2018**, *9*, 2723.

- (37) Diep, B. A.; Gill, S. R.; Chang, R. F.; Phan, T. H.; Chen, J. H.; Davidson, M. G.; Lin, F.; Lin, J.; Carleton, H. A.; Mongodin, E. F. Complete genome sequence of USA300, an epidemic clone of community-acquired meticillin-resistant Staphylococcus aureus. *Lancet* 2006, 367 (9512), 731–739.
- (38) Lim, S.; Lee, W.; Na, S.; Shin, J.; Lee, Y. N-nitrosodimethylamine (NDMA) formation during ozonation of N,N-dimethylhydrazine compounds: Reaction kinetics, mechanisms, and implications for NDMA formation control. *Water Res.* **2016**, *105*, 119–128.
- (39) ATCC, Staphylococcus aureus subsp. aureus Rosenbach (ATCC® BAA-1556) In.
- (40) Monecke, S.; Coombs, G.; Shore, A. C.; Coleman, D. C.; Akpaka, P.; Borg, M.; Chow, H.; Ip, M.; Jatzwauk, L.; Jonas, D.; Kadlec, K.; Kearns, A.; Laurent, F.; O'Brien, F. G.; Pearson, J.; Ruppelt, A.; Schwarz, S.; Scicluna, E.; Slickers, P.; Tan, H.-L.; Weber, S.; Ehricht, R. A Field Guide to Pandemic, Epidemic and Sporadic Clones of Methicillin-Resistant Staphylococcus aureus. *PLoS One* **2011**, *6* (4), e17936.
- (41) biomedicals, M. Crushing Lysis Efficiency. Nothing Resists FastPrep®. https://www.mpbio.com/media/productattachment/LS042019-EN-Sample-Preparation-Brochure.pdf.
- (42) He, H.; Wu, S. J.; Fang, X.; Anderson, A. K.; Roberts, M. C.; Lee, Y.; Dodd, M. C., Application of kinetics-based modeling approaches to predicting antibiotic resistance gene degradation during UV-and chlorine-based wastewater disinfection processes: from bench-scale to full-scale. *In preparation*.
- (43) Pinkernell, U.; Nowack, B.; Gallard, H.; Von Gunten, U. Methods for the photometric determination of reactive bromine and chlorine species with ABTS. *Water Res.* **2000**, *34* (18), 4343–4350.
- (44) Forsyth, J. E.; Zhou, P.; Mao, Q.; Asato, S. S.; Meschke, J. S.; Dodd, M. C. Enhanced inactivation of Bacillus subtilis spores during solar photolysis of free available chlorine. *Environ. Sci. Technol.* **2013**, 47 (22), 12976–12984.
- (45) Canonica, S.; Meunier, L.; Von Gunten, U. Phototransformation of selected pharmaceuticals during UV treatment of drinking water. *Water Res.* **2008**, *42* (1), 121–128.
- (46) Volkmann, H.; Schwartz, T.; Bischoff, P.; Kirchen, S.; Obst, U. Detection of clinically relevant antibiotic-resistance genes in municipal wastewater using real-time PCR (TaqMan). *J. Microbiol. Methods* **2004**, *56* (2), 277–286.
- (47) Oliveira, D. C.; de Lencastre, H. Multiplex PCR strategy for rapid identification of structural types and variants of the mec element in methicillin-resistant Staphylococcus aureus. *Antimicrob. Agents Chemother.* **2002**, *46* (7), 2155–2161.
- (48) Lee, Y.; Imminger, S.; Czekalski, N.; Von Gunten, U.; Hammes, F. Inactivation efficiency of Escherichia coli and autochthonous bacteria during ozonation of municipal wastewater effluents quantified with flow cytometry and adenosine tri-phosphate analyses. *Water Res.* **2016**, *101*, 617–627.
- (49) Murtey, M. D.; Ramasamy, P., Sample preparations for scanning electron microscopy—life sciences. In *Modern electron microscopy in physical and life sciences*; IntechOpen: 2016.
- (50) Deborde, M.; Von Gunten, U. Reactions of chlorine with inorganic and organic compounds during water treatment—kinetics and mechanisms: a critical review. *Water Res.* **2008**, *42* (1), 13–51.
- (51) Theruvathu, J. A.; Flyunt, R.; Aravindakumar, C. T.; von Sonntag, C. Rate constants of ozone reactions with DNA, its constituents and related compounds. *Journal of the Chemical Society, Perkin Transactions* 2 **2001**, *3*, 269–274.
- (52) Van der Zee, J.; Dubbelman, T.; Steveninck, J. V. The role of hydroxyl radicals in the degradation of DNA by ozone. *Free Radical Res. Commun.* **1987**, 2 (4–6), 279–284.
- (53) Douki, T.; Cadet, J. Individual determination of the yield of the main UV-induced dimeric pyrimidine photoproducts in DNA suggests a high mutagenicity of CC photolesions. *Biochemistry* **2001**, *40* (8), 2495–2501.
- (54) Holman, M. R.; Ito, T.; Rokita, S. E. Self-repair of thymine dimer in duplex DNA. *J. Am. Chem. Soc.* **2007**, *129* (1), 6–7.

- (55) Law, Y. K.; Forties, R. A.; Liu, X.; Poirier, M. G.; Kohler, B. Sequence-dependent thymine dimer formation and photoreversal rates in double-stranded DNA. *Photochemical & Photobiological Sciences* **2013**, *12* (8), 1431–1439.
- (56) Sinha, R. P.; Häder, D.-P. UV-induced DNA damage and repair: a review. *Photochemical & Photobiological Sciences* **2002**, *1* (4), 225–236.
- (57) Pecson, B. M.; Ackermann, M.; Kohn, T. Framework for Using Quantitative PCR as a Nonculture Based Method To Estimate Virus Infectivity. *Environ. Sci. Technol.* **2011**, *45* (6), 2257–2263.
- (58) Cadet, J.; Douki, T. Formation of UV-induced DNA damage contributing to skin cancer development. *Photochemical & Photobiological Sciences* **2018**, *17* (12), 1816–1841.
- (59) Prutz, W. A. Hypochlorous acid interactions with thiols, nucleotides, DNA, and other biological substrates. *Arch. Biochem. Biophys.* **1996**, 332 (1), 110–120.
- (60) Sugiyama, H.; Saito, I. Theoretical studies of GG-specific photocleavage of DNA via electron transfer: significant lowering of ionization potential and 5'-localization of HOMO of stacked GG bases in B-Form DNA. *J. Am. Chem. Soc.* **1996**, *118* (30), 7063–7068.
- (61) Geeraerd, A.; Valdramidis, V.; Van Impe, J. GInaFiT, a freeware tool to assess non-log-linear microbial survivor curves. *Int. J. Food Microbiol.* **2005**, *102* (1), 95–105.
- (62) Dodd, M. C. Potential impacts of disinfection processes on elimination and deactivation of antibiotic resistance genes during water and wastewater treatment. *J. Environ. Monit.* **2012**, *14* (7), 1754–1771.
- (63) Cho, M.; Kim, J.; Kim, J. Y.; Yoon, J.; Kim, J.-H. Mechanisms of Escherichia coli inactivation by several disinfectants. *Water Res.* **2010**, 44 (11), 3410–3418.
- (64) Ramseier, M. K.; von Gunten, U.; Freihofer, P.; Hammes, F. Kinetics of membrane damage to high (HNA) and low (LNA) nucleic acid bacterial clusters in drinking water by ozone, chlorine, chlorine dioxide, monochloramine, ferrate(VI), and permanganate. *Water Res.* **2011**, *45* (3), 1490–1500.
- (65) Tretyakova, N. Y.; Groehler, A., IV; Ji, S. DNA-protein crosslinks: formation, structural identities, and biological outcomes. *Acc. Chem. Res.* **2015**, 48 (6), 1631–1644.
- (66) Loegager, T.; Holcman, J.; Sehested, K.; Pedersen, T. Oxidation of ferrous ions by ozone in acidic solutions. *Inorg. Chem.* **1992**, *31* (17), 3523–3529.
- (67) Pestovsky, O.; Bakac, A. Reactivity of Aqueous Fe(IV) in Hydride and Hydrogen Atom Transfer Reactions. *J. Am. Chem. Soc.* **2004**, 126 (42), 13757–13764.
- (68) Park, S.; Imlay, J. A. High Levels of Intracellular Cysteine Promote Oxidative DNA Damage by Driving the Fenton Reaction. *J. Bacteriol.* **2003**, *185* (6), 1942.
- (69) Haaber, J.; Cohn, M. T.; Frees, D.; Andersen, T. J.; Ingmer, H. Planktonic Aggregates of Staphylococcus aureus Protect against Common Antibiotics. *PLoS One* **2012**, *7* (7), e41075.
- (70) Bohrerova, Z.; Linden, K. G. Ultraviolet and Chlorine Disinfection of Mycobacterium in Wastewater: Effect of Aggregation. *Water Environ. Res.* **2006**, 78 (6), 565–571.
- (71) Mamane, H.; Linden, K. G. Impact of particle aggregated microbes on UV disinfection. I: evaluation of spore—clay aggregates and suspended spores. *J. Environ. Eng.* **2006**, 132 (6), 596–606.
- (72) Dietrich, J. P.; Loge, F. J.; Ginn, T. R.; Başağaoğlu, H. Inactivation of particle-associated microorganisms in wastewater disinfection: Modeling of ozone and chlorine reactive diffusive transport in polydispersed suspensions. *Water Res.* **2007**, *41* (10), 2189–2201.
- (73) Ray, M.; Boundy, S.; Archer, G. Transfer of the methicillin resistance genomic island among staphylococci by conjugation. *Mol. Microbiol.* **2016**, *100* (4), 675–685.
- (74) Chlebowicz, M. A.; Mašlaňová, I.; Kuntová, L.; Grundmann, H.; Pantůček, R.; Doškař, J.; van Dijl, J. M.; Buist, G. The Staphylococcal Cassette Chromosome mec type V from Staphylococcus aureus ST398 is packaged into bacteriophage capsids. *Int. J. Med. Microbiol.* **2014**, 304 (5–6), 764–774.

- (75) Haaber, J.; Leisner, J. J.; Cohn, M. T.; Catalan-Moreno, A.; Nielsen, J. B.; Westh, H.; Penadés, J. R.; Ingmer, H. Bacterial viruses enable their host to acquire antibiotic resistance genes from neighbouring cells. *Nat. Commun.* **2016**, 7 (1), 1–8.
- (76) Morikawa, K.; Takemura, A. J.; Inose, Y.; Tsai, M.; Thi, L. T. N.; Ohta, T.; Msadek, T. Expression of a cryptic secondary sigma factor gene unveils natural competence for DNA transformation in Staphylococcus aureus. *PLoS Pathog.* **2012**, *8* (11), e1003003.